Rock Mechanics and Rock Engineering
https://doi.org/10.1007/s00603-019-01813-9

TECHNICAL NOTE

A Hydro-fracturing Tester for Rock Saturated with Controlled Two-Phase Pore Fluids

Bing Bai[1,2] · **Chenyu Xu**[3] · **Mingze Liu**[1] · **Xiaochun Li**[1]

Received: 2 September 2017 / Accepted: 5 April 2019

Keywords Hollow cylinder · Unsaturated hydraulic fracturing tester · Two-phase fracturing · CO_2–water two-phase fluids

1 Introduction

In recent years, an increasing number of engineering operations related to underground fluid injection have appeared. These involve fields like not only traditional oil and gas recovery, but also some unconventional engineering such as CO_2 geological storage (Metz et al. 2005; Holtz et al. 2001; Spycher and Pruess 2010; Rogala et al. 2013) and acid gas re-injection (Chakma 1997). In some of these processes, the injection pressure should be controlled to prevent the fracturing of the formations to ensure the mechanical stability of sites (Hawkes et al. 2005; Li et al. 2014; Rutqvist and Tsang 2002; Streit and Hillis 2004). In some others, artificial fracturing is usually required to improve the permeability of the reservoirs. In many occasions such as CO_2 fracturing or injection, the formations are actually saturated with two-phase pore fluids. Accordingly, one of the common issues in such processes is the hydro-fracturing failure behavior of the formation rocks under the action of gas–water mixtures, which might be significantly different from that under a single-phase fluid. The hydro-fracturing failure behavior of rocks under this condition would be influenced by effects of partial pressures, the change of pore flow, and the physical and chemical reactions between the fluids and rocks. Therefore, a hydro-fracturing device and the test method for rocks saturated with controlled two-phase pore fluids are valuable for the experimental investigations.

The surrounding rocks at the bottom hole are generally under a true triaxial stress state with a negative minimum principal stress (Matthews and Kelly 1967). In the existing test techniques, the method based on the hollow cylinder could implement similar stress state on the specimen by imposing the axial, the confining, and the internal pressures. A series of this type of test devices have been developed since the first hollow cylinder testing device for splitting tests of sandstone by F. D. Adams (Adams 1912; Jingnong and Mianba 1986; Périépj 1990; Lee et al. 1999; Song et al. 2001; Kanj et al. 2003; Monfared et al. 2011). Moreover, many investigations of mechanical behaviors of rocks have been conducted by researchers by the hollow cylinder tester (Zhang et al. 2010; You et al. 2010). Therefore, the hollow cylinder test method has been actually widely used. However, none of the existing hollow cylinder-based testers is capable of testing the hydro-fracturing behavior of rocks saturated with controlled two-phase fluids.

In this work, the traditional hollow cylinder tester was upgraded to make a novel hydro-fracturing tester for rocks saturated with controlled two-phase fluids to meet many new emerging needs as mentioned previously. One of the highlights of this device is the additional function of saturation control of the gas–water pore mixtures in the rock specimen. The controlled stress state is built the same way as the traditional hollow cylinder tester, while the two-phase pore fluids are controlled to form specific partial pressure or saturation.

✉ Bing Bai
bai_bing2@126.com

[1] State Key Laboratory of Geomechanics and Geotechnical Engineering, Institute of Rock and Soil Mechanics, Chinese Academy of Sciences, Wuhan 430071, China

[2] Hubei Key Laboratory of Environmental Geotechnology, Institute of Rock and Soil Mechanics, Chinese Academy of Sciences, Wuhan 430071, China

[3] School of Civil Engineering, Architechture and Environment, Hubei University of Technology, Wuhan 430068, Hubei, China

Published online: 26 April 2019

2 Design and Implementation

The structure of the device is shown in Fig. 1a, b which shows the manufactured test system. The device consists of five parts, namely a triaxial loading subsystem, a two-phase fluid controlling subsystem, a pressure chamber, a data acquisition subsystem, and a temperature controlling subsystem. The steel tubes with an external diameter of 3.18 mm (1/8 ft) and an internal diameter of 0.9 mm were used as the pipelines. Both cutting ferrules and thread jointers were used for connections. Needle valves and ball valves were used as the control valves. The device can function at a maximum pressure of 50 MPa. Considering the end frictional effects between the sample and the lower pad may greatly affect the test results (Hao et al. 2013), copper sheet and polytetrafluoroethylene (PTFE) film were used to reduce the end friction. Particularly, the copper sheet was pressed against the end of the sample, while the PTFE film touched the end of the pad. In the next paragraphs, the primary parts of the device are detailed as follows.

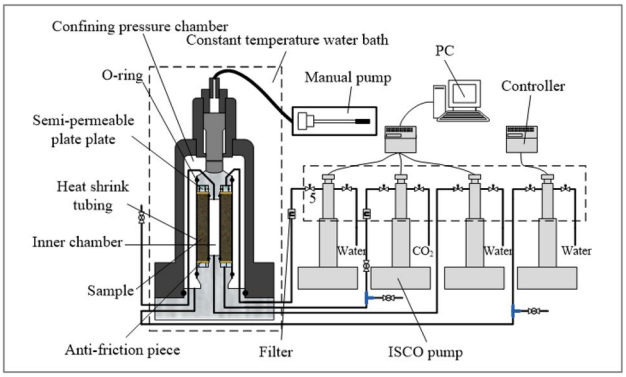

(a) The structure of the test device（Liu and Bai et al. 2016b)

(b) The manufactured test system

Fig. 1 The test device

2.1 Triaxial Loading Subsystem

The triaxial loading subsystem, the basic principle of which is the same as the traditional hydro-fracturing tester based on hollow cylinder specimen, was implemented by combining two metering pumps (ISCO 100D and ISCO 500D) and a manual hydraulic pump, which were used for the loading of internal pressure, confining pressure, and axial pressure, respectively. Both pressure and flow rate can be accurately controlled by the metering pumps. Moreover, the pressure, flow rate, and volume of fluid can be recorded in real time. The internal pressure pump had a pressure controlling range of 0–68.95 MPa and a flow range of 0.01×10^{-3}–50 mL/min, while both parameters had a controlling precision of 0.5%. The internal pressure was applied by pumping the fluid into the inner chamber of the sample through the channels on the device's base plate, while the air in the inner chamber can be discharged through the channels from the upper pad to the base plate. The confining pressure pump had a pressure controlling range of 0–25.86 MPa and a flow range of 1.0×10^{-3}–204 mL/min, while both parameters were controlled with a precision of 0.5%. The confining pressure was applied by pumping the fluid into the confining pressure chamber through the channels on the base plate. The manual hydraulic pump had a pressure range of 0–50 MPa. The axial pressure on the sample's upper surface was loaded using the manual pump through the jack on the top of the pressure chamber.

2.2 Pore-Fluid Subsystem

The pore-fluid subsystem mainly consists of two metering pumps (ISCO 260D) and a semi-permeable plate. These two metering pumps are used for controlling of pore water and pore CO_2. The pressure controlling range is 0–51.71 MPa with a precision of 0.5%, while the flow rate controlling range is 1.0×10^{-3}–107 mL/min with a precision of 0.5%. After being preprocessed, the semi-permeable plate was embedded in the circular holes on the upper pad, as shown in Fig. 2a, b. Its entry pressure for the non-wetting phase is 1.5 MPa, which means that when the pressure difference between the gas and the liquid in the rock pores is lower than 1.5 MPa, the gas cannot pass through the plate, while the water can. During the fracturing tests of two-phase pore fluids, the partial saturations and pressures were controlled using this subsystem. First, the rock sample and the semi-permeable plate were fully saturated with water. Then, the gas was pumped into the sample using the metering pump through the channel in the lower plate. When being pumped into the rock sample,

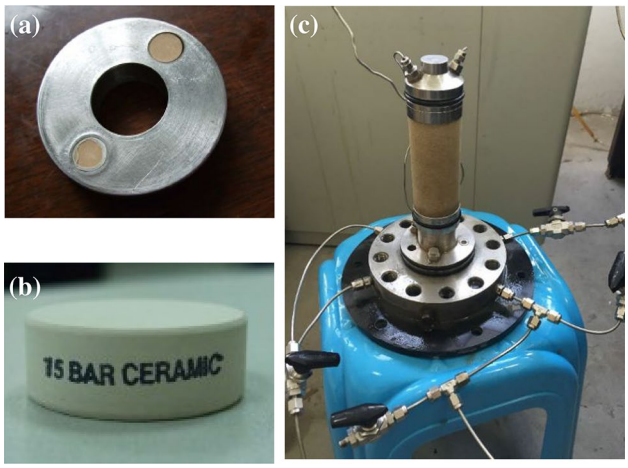

Fig. 2 The inside of the pressure chamber. **a** Semi-permeable plate; **b** the upper pad after the embedding the semi-permeable plate. **c** The pressure chamber before installation of top hood and specimen

the gas would drive and discharge the pore water into the metering pump through the plate. During the tests, the pressure difference between the gas and the water was controlled to be smaller than the entry pressure. Therefore, the gas would be blocked by the plate. During the driving process, the saturation of the gas increased gradually. Therefore, the capillary force, which the gas should overcome to enter the rock pores, increased too. When the capillary force increased to a value larger than the applied pressure, the gas would no longer enter the rock and, thus, stop the displacement. The saturation of the gas in the rock after the displacement can be calculated based on the displacement water using the following equation:

$$S_{\text{gas}} = \frac{V_{\text{af}} - V_{\text{be}}}{V_{\text{p}}} \times 100\% \tag{1}$$

where V_{af} denotes the volume recorded by the metering pump after the displacement (ml), V_{be} denotes the volume recorded by the metering pump before the displacement (ml), and V_{p} denotes the volume of the sample pores (ml).

2.3 Pressure Chamber

Figure 1a shows the structure of the pressure chamber in the test device. The manufactured test system is shown in Fig. 1b. The pressure chamber consists of a top hood, a specimen holder, and multiple fluid channels. The upper and lower ends of the hollow sample are connected to the pumps on the upper pad and the lower foundation support, respectively. Thus, the sample can be fixed in the center of the pressure chamber. If necessary, the space among the confining fluid, the internal pressure fluid, and the sample can be sealed using the Teflon heat-shrinkable tubes and O-shape rings. Figure 2 shows the inside view of the pressure chamber.

2.4 Temperature Control and Data Acquisition

The temperature control subsystem includes a constant-temperature water bath and an external circulator bath. The pressure chamber is put in the water bath for heating and maintaining a constant temperature, while the constant-temperature water can be circulated to the constant-temperature chamber in the metering pump for achieving the constant temperature of the fluid in the metering pump. The water bath temperature is monitored by the temperature-sensing platinum resistor in the constant-temperature water bath, such that the output power of the heater can be controlled, which, in turn, maintains the temperature at a given value within the range of 10–95 °C. The fluctuation of the temperature is less than 0.1 °C. The constant-temperature water bath can display the real-time values of the temperature.

The data acquisition subsystem includes a pressure gauge of the manual oil hydraulic pump, a water bath thermometer, a pressure sensor, a flow sensor, a volume sensor on the metering pump, and the data acquisition software. The pressure sensor, the flow rate sensor, and the volume sensor were installed on the top of the ISCO metering pump, which could collect real-time data of the metering pump's pressure, flow rate, and volume at a sampling frequency of 2 Hz. The acquired data were transmitted to the computer, and then recorded in real time by the control software embedded in the ISCO pump.

3 Function Tests

The basic function of the tester was preliminarily demonstrated in some early experimental studies of sandstone under CO_2–water conditions (Liu et al. 2016a, b). In this section, two new experiments are presented to further demonstrate and validate the functions of the test facility independently. The engineering background of both experiments comes from geological storage of carbon dioxide. During the injection process, CO_2 displaces the formation of water forming two-phase pore flow of CO_2 and brine in the rock formations. The partial pressure or saturation of CO_2 is usually not uniformly distributed in the reservoir, which would affect the fracturing behavior of the formation rocks. The first experiment is to demonstrate the control of two-phase pore fluids in a rock specimen, which is a critical link to conduct the hydro-fracturing tests. In the second experiment, a hydro-fracturing test of sandstone considering CO_2 infiltration into the rock is presented to fully show the hydro-fracturing function involved in controlled two-phase pore fluids.

3.1 CO_2/Water Displacement in Sandstone

3.1.1 Specimen and Test Scheme

The sandstone with sound homogeneity was used in this test, which was sampled from Zigong, Sichuan province, China. Figure 3 shows the rock specimen used in the current work. The porosity and permeability of the specimen were 10.16% and 4.35 mD, respectively. According to the X-ray diffraction tests, the sample contained 97.73% silica, 1.82% kaolinite, and 0.45% sodalite. The mercury injection test results revealed that the pore diameter was 10 μm.

The whole test included the sample installation, water saturation, CO_2 displacement, and fracturing the specimen. The specific test procedures were described By Liu et al. (2016a).

3.1.2 Saturation Control

For this tester, the control of overall saturation of CO_2 in rock specimen could be indirectly implemented by controlling the displacement pressures of CO_2 and water. The rock specimen is initially saturated with water of a given pressure P_1 at the outlet side. Then, CO_2 is injected into the inlet side of the rock specimen at pressure P_2 and CO_2 will displace the water. Because of the blocking effect of semi-permeable plate on CO2 (Fig. 2a), only water will come out of the rock specimen. With the continuous displacement, the CO_2 saturation will gradually increase and the capillary resistance to be overcome will also increase. When the capillary resistance increases to a value greater than the pressure difference (P_2–P_1) between CO_2 and water, the displacement will stop and the overall saturation of CO_2 will be maintained. At this moment, the overall saturation of CO_2 could be obtained by the recorded amount of water discharged.

Fig. 3 The sandstone sample

3.1.3 Water Displacement by CO_2

Three groups of fracturing tests in two-phase fluids of CO_2 and water were conducted, where the pressure of CO_2 was set at 3.0 MPa, 3.4 MPa, and 3.7 MPa, respectively. The water pressure was set at 2.5 MPa, while the axial and the confining stresses were 2.5 MPa and 20 MPa, respectively. The temperature was set to 25 °C.

Figure 4 shows the pressure variation of the pore water pump with time during the displacement process under the CO_2 pressure of 3.0 MPa. It can be observed that the whole displacement process has three stages. First, at $t = 5732$ s, the valve was switched on. The CO_2 began to enter the rock and the pore water pressure increased suddenly. Then, at $t = 5752$ s, the pore water pressure reached a maximum value of 2.60 MPa, which then decreased rapidly and tended to stabilize because of the adjustment of the metering pump's constant-pressure mode. During this stage, the pressure and the flux rate were not stable, indicating that this stage was an unstable displacement stage and lasted for 30 s in total. The appearance of this unstable displacement state might be due to the fact that the water in the system's dead volume and the rock's large-scale pores would be first and quickly displaced by CO_2. Next, the pore water pressure remained at a relatively stable level of approximately 2.50 MPa, indicating that this stage was a stable displacement stage and lasted for 18.92 h. Finally, the displacement stopped at $t = 20.32$ h. At this stage, the pore water returned to the preset pressure value (2.50 MPa) and was no longer displaced.

Figure 5 shows the relationship between the CO_2 saturation after the displacement and the displacement pressure for each test. It can be observed that the CO_2 saturation after the displacement range from 44.15% to 68.43%, i.e., the CO_2 saturation goes up with the increase of CO_2 displacement pressure. This is because higher pressure could make CO_2 enter more rock pores and displace more water.

3.2 Hydraulic Fracturing Test of Sandstone Considering CO_2 Infiltration

After being injected into the formation, CO_2 would infiltrate the pores in the formation rocks and displace the pre-existing water. The CO_2 infiltration process would lead to seepage force which might contribute to formation fracturing. The seepage force shows some differences from the traditional seepage force of water due to the larger compressibility and lower viscosity of CO_2. However, this has still been poorly investigated and understood. The fracturing tests on the porous media induced by the infiltration of fluid can be carried out using the current device.

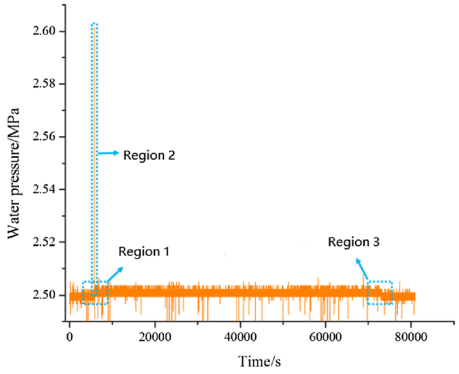

(a) Overall variation of pump water pressure with time

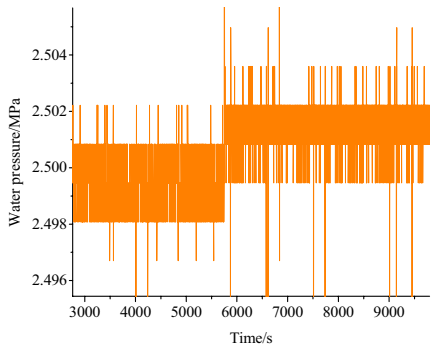

(b) Magnification view of region 1 of Fig. (a)

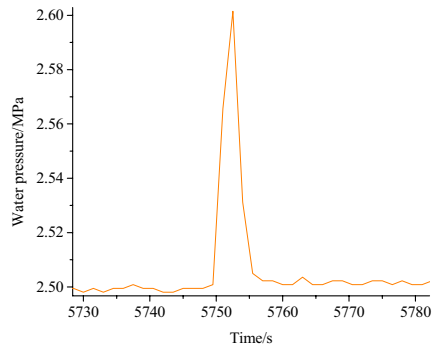

(c) Magnification view of region 2 of Fig. (a)

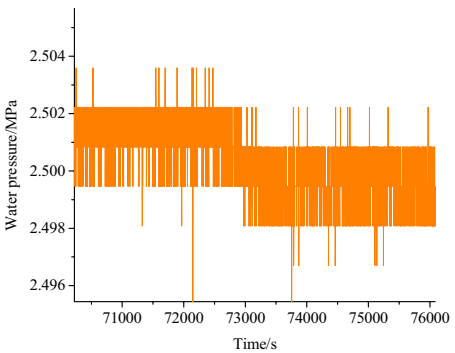

(d) Magnification view of region 3 of Fig. (a)

Fig. 4 Variation of the pore water pressure with time during the CO_2/water displacing process

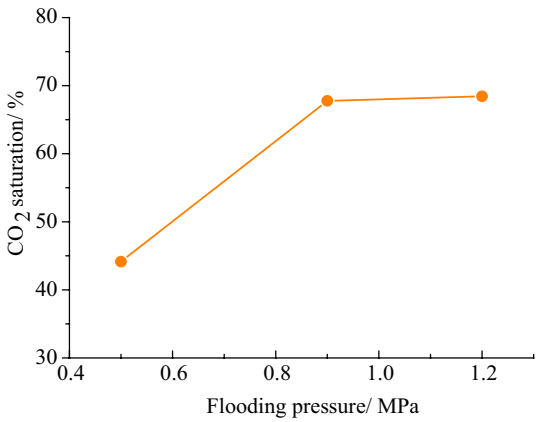

Fig. 5 Relationship between the calculated CO_2 saturation and flooding pressure in the CO_2 flooding step

3.2.1 Test Sample and Scheme

To accumulate sufficient internal pressure to make the fracturing take place in the experiment, the rock specimen with low permeability is preferred. Figure 6 shows the sandstone specimen used in the current tests. The selected sandstone sample has a permeability of 0.0069 mD, and is composed of 59.38% quartz, 9.66% kaolinite, 7.87% calcite, 7.57% dolomite, 7.41% albite, 5.23% illite, and 2.88% chlorite according to the X-ray diffraction test.

Most of the specific test procedures were described in the previous sessions. The difference is, in this test, that the sample was not surrounded with the heat shrinkable sleeve inside the rock hole, and thus, the inner chamber, the rock pores, and the confining pressure were interconnected. When being injected into the inner pressure chamber, the CO_2 was infiltrated into the sample's pores and then displaced the pre-existing water into the confining pressure chamber. In this test, CO_2 was injected into the sample which was pre-saturated with 10 MPa pore water at a rate of 20 ml/min to fracture the rock specimen. As the rock pores were directly

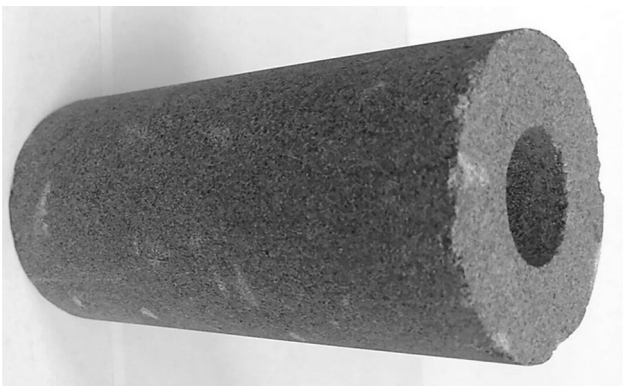

Fig. 6 Sandstone used in the infiltration-induced fracturing tests

connected to the confining pressure chamber, the confining pressure was also 10 MPa. In addition, both the pore pressure and the confining pressure were controlled by the metering pump in a constant-pressure mode.

3.2.2 Test Results

Figure 7 shows the variations in internal pressure and confining pressure with time at a water injection rate of 20ml/min. The orange curve in this figure denotes the variation of internal pressure. It can be observed that, after the fluid was injected, the internal pressure increased gradually from the initial pressure of 10 MPa. This can be attributed to the rock's low permeability. In other words, the injected fluid cannot dissipate outwards rapidly through the rock sample, thus leading to the increase of pressure. At 76 s, the internal pressure reached up to 13.7 MPa and then suddenly dropped to 12.3 MPa. This is because, at this moment, the sample was fractured and the interconnected fractures were produced from the sample's internal wall to the external wall. Therefore, the permeability increased suddenly, and a significant amount of the internal fluid ran off, leading to the sudden decrease of the internal pressure. Accordingly, the peak pressure of the curve can be regarded as the sample's fracturing pressure. The purple curve in this figure denotes the variation of confining pressure. The confining pressure showed no significant variation before fracturing because of the constant-pressure mode of the pump was set. Due to the breakdown of the sample at 76 s, significant amount of the internal fluid flowed into the confining pressure chamber through the sample, leading to a sudden increase in the confining pressure to 12.3 MPa. Although the volume of the fluid in the confining pressure chamber exceeded that in the inner chamber, as the compressibility of CO_2 in the internal pressure chamber is much greater than that of water in the confining pressure chamber, the sudden increase in the confining pressure was larger than the sudden decrease of the internal pressure. It can also be observed from the figure that, after breakdown, the internal pressure was almost equal to the confining pressure. This is due to the fact that the pressure drop of the CO_2 leaked to the confining chamber is not notable, because the viscosity of CO_2 is small and, the flow resistance is therefore very small, too.

Figure 8 shows the variations in flow rates of the internal pressure pump and confining pressure pump during the test. The orange curve denotes the variation in the internal pressure pump flow rate, while the purple curve denotes the variation in the confining pressure pump flow rate. During the water injection process, the injected flow rate of the metering pump was set at 20 ml/min in a constant rate mode. As the confining pump was operated in a constant-pressure mode, when the CO_2 flowed into the confining pressure chamber through the sample during the fracturing, the piston was moved back by the pump for stabilizing the pressure, thus yielding negative flow rate. When the difference between the pressure of the confining pump and the preset value was increased, larger flow rate for pressure balance was required. Therefore, the flow rate of the confining pump represented the fluid's seepage velocity from the inner chamber to the confining chamber. During the process that the CO_2 displaced the water in the specimen pores, the flow is impeded by the capillary force and the water driven to the confining pressure chamber was very limited. Therefore, it was difficult to cause the large movement of the piston in the confining pressure pump. Therefore, the flow rate–time

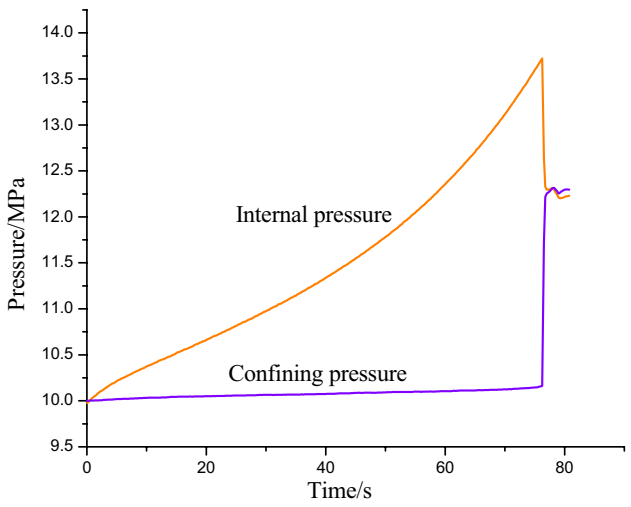

Fig. 7 Variations in internal pressure and confining pressure with time during the sample fracturing (CO_2-injection rate: 20 ml/min)

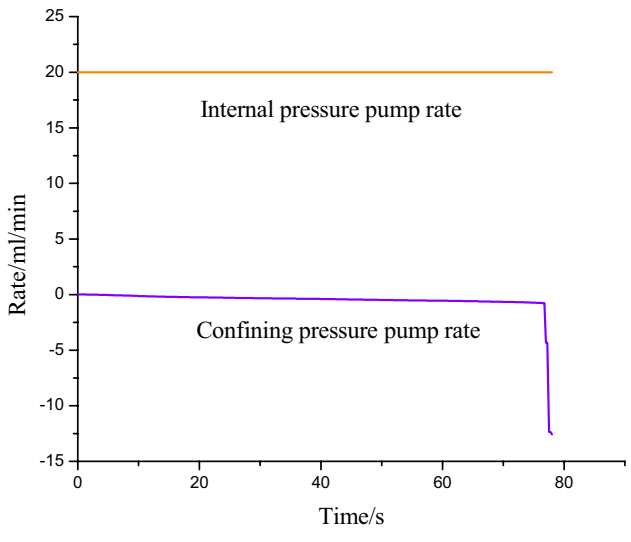

Fig. 8 Variations in the internal pressure pump rate and confining pressure pump rate with time during the fracturing process (CO_2-injection rate: 20 ml/min)

curve of the internal pressure pump was almost steady for a long time, which can be seen from the figure. It can also be seen from the figure that the flow rate of the confining pump suddenly increases from 0 ml/min to 12.24 ml/min at 76 s. This is because the breakdown of the sample caused much of the CO_2 to flow into the confining pressure chamber, making the flow rate of the confining pressure pump in the constant-pressure mode increase sharply to regulate the confining pressure.

3.3 Short Discussion

Although the control of the overall saturation of the gas–water pore mixtures in the rock specimen was effectively implemented and two types of hydraulic fracturing tests were, therefore, successfully conducted, the test work was still preliminary, and further experimental investigations are required. First, we do not have the test condition to obtain the actual distribution of water–CO_2 mixture along the rock sample. However, as flooding is a slow process and the cease of it needs good homogeneity of fluid pressure in the rock sample, it might be reasonable to consider that the water–CO_2 mixture also has good homogeneity when the flooding ceased. Second, in each test, the observed crack in the rock sample after fracturing is approximately vertical and quite similar. We changed the pore pressure and fluid type in each experiment and found that they seemed to remarkably influence the fracturing pressure rather than the crack pattern. Therefore, the crack patterns depend much more on the stress state than the saturation of water–CO_2 mixture in the rock sample. However, this is a quite preliminary observation based on limited tests, and the effect of saturation and its distribution on the crack patterns is a valuable question that requires much more experimental work in future, especially combining the analysis of material properties related to fracturing process.

4 Conclusions

This study presented a novel hydro-fracturing tester for rocks. One of the highlights of this new device is the function of saturation control of the gas–water pore mixtures in the rock specimen. The device actually provides a powerful means to study the mechanical behavior of rocks under multi-physics conditions. The test principle, design considerations, and the main components of the device were first detailed. The main functions and effectiveness of the device were demonstrated with three typical tests. The device has been proved to have outstanding repeatability and reliability. Hydraulic fracturing tests of sandstones (saturated with CO_2 and water, and considering CO_2 infiltration) clearly show the novel functions of the new device are successful achieved. In addition, it is worth noting that the developed equipment can not only accomplish the traditional and the two-phase hydraulic fracturing experiments, but also conduct a variety of other kinds of experiments with minor modifications. For example, permeability tests, capillary curves tests, and fracturing-seepage coupling tests, etc. Therefore, this device can serve as an fundamental platform for various advanced tests.

Acknowledgements The authors gratefully acknowledge the support of this work by the National Natural Science Foundation of China (Grant No. 41672252), the Program of International Science and Technology Cooperation, China (Grant No. S2016G9005), and the National Key Technology Support Program of China (Grant No. 2014BAC18B01).

Compliance with ethical standards

Conflicts of Interest The authors declare no conflict of interest.

References

Adams FD (1912) An experimental contribution to the question of the depth of the zone of flow in the earth's crust. J Geol 20(2):97–118

Alsayed M (2002) Utilising the hoek triaxial cell for multiaxial testing of hollow rock cylinders. Int J Rock Mech Min Sci 39(3):355–366

Chakma A (1997) Acid gas re-injection—a practical way to eliminate CO_2 emissions from gas processing plants. Energy Convers Manag 38:S205–S209

Hao Y, Hao H, Li Z (2013) Influence of end friction confinement on impact tests of concrete material at high strain rate. Int J Impact Eng 60:82–106

Hawkes C, McLellan P, Bachu S (2005) Geomechanical factors affecting geological storage of CO_2 in depleted oil and gas reservoirs. J Can Petrol Technol 44(10):2005

Holtz MH, Nance PK, Finley RJ (2001) Reduction of greenhouse gas emissions through CO_2 Eor in Texas. Environ Geosci 8(3):187–199

Houquan Z (2010) Study on ringlike splitting failure and its related mechanical behavior of rock cylinders under unloading condition after high compression. China University of Mining and Technology, Xuzhou, Ph.D.thesis

Jingnong W, Mianba W (1986) Experimental research of rock fracture under pore-traixial stress condition. Seismol Geol 8(2):69–76

Kanj M, Abousleiman Y, Ghanem R (2003) Poromechanics of anisotropic hollow cylinders. J Eng Mech 129(11):1277–1287

Lee D-H, Juang CH, Chen J-W, Lin H-M, Shieh W-H (1999) Stress paths and mechanical behavior of a sandstone in hollow cylinder tests. Int J Rock Mech Min Sci 36(7):857–870

Li Q, Fei W, Liu X, Wei X, Jing M, Li X (2014) Challenging combination of CO_2 geological storage and coal mining in the Ordos Basin, China. Greenh Gases Sci Technol 4(4):452–467

Liu M, Bai B, Li X, Gao S, Wang L, Wu H (2016a) Experimental study of fracturing characteristics of sandstone under CO_2-water two-phase condition and effective stress model. Chin J Rock Mech Eng 35(2):250–259

Liu M, Bai B, Li X, Gao S, Wang L, Wu H (2016b) Assessing the applicability of unsaturated effective stress models to tensile fracturing of sandstone in CO_2–water two-phase fluids. Greenhouse Gases Sci Technol 6(5):670–681

Matthews W, Kelly J (1967) How to predict formation pressure and fracture gradient. Oil Gas J 65(8):92–106

Metz B, Davidson O, De Coninck H, Loos M, Meyer L (2005) Ipcc Special Report on Carbon Dioxide Capture and Storage. Working Group III, Intergovernmental Panel on Climate Change, Geneva (Switzerland)

Monfared M, Delage P, Sulem J, Mohajerani M, Tang AM, De Laure E (2011) A new hollow cylinder triaxial cell to study the behavior of geo-materials with low permeability. Int J Rock Mech Min Sci 48(4):637–649

PÉRIÉPJ (1990) Laboratory Investigation of Rock Fracture on Borehole. University of California, Berkeley, USA, Ph.D.thesis

Rogala A, Krzysiek J, Bernaciak M, Hupka J (2013) Non-aqueous fracturing technologies for shale gas recovery. Physicochem Probl Mineral Process 49(1):313–322

Rutqvist J, Tsang C-F (2002) A study of caprock hydromechanical changes associated with CO_2-injection into a brine formation. Environ Geol 42(2–3):296–305

Song I, Suh M, Won KS, Haimson B (2001) A laboratory study of hydraulic fracturing breakdown pressure in tablerock sandstone. Geosci J 5(3):263–271

Spycher N, Pruess K (2010) A Phase-partitioning model for CO_2–brine mixtures at elevated temperatures and pressures: application to CO_2-enhanced geothermal systems. Transp Porous Media 82(1):173–196

Streit JE, Hillis RR (2004) Estimating fault stability and sustainable fluid pressures for underground storage of CO_2 in Porous Rock. Energy 29(9):1445–1456

You M, Su C (2010) Study of strength and failure of hollow cylinders and rings of sandstone under compression-tension stresses. Chin J Rock Mech Eng 6: 004